Journal of Computers Vol. 30 No. 3, 2019, pp. 290-304
doi:10.3966/199115992019063003024

High-accuracy 3D indoor Positioning Algorithm Based on P440 Ultra-wideband Ranging and Communication Module

Hui Liu[1*], Xu Zhang[1], Lei Zhang[1], Lei Pang[2,3], Fang Li[1]

[1] Department of Automation, Beijing University of Civil Engineering and Architecture, Beijing 100044, China
{liuhui, zhanglei, lifang}@bucea.edu.cn; zhangxu13@foxmail.com

[2] Department of Remote Sensing, Beijing University of Civil Engineering and Architecture, Beijing 100044, China
panglei@bucea.edu.cn

[3] Department of Earth Observation Data Science, German Aerospace Center (DLR), Germany
panglei@bucea.edu.cn

Received 1 March 2019; Revised 8 April 2019; Accepted 7 May 2019

Abstract. Many indoor mobile robotic applications require knowledge of the exact robot location within the work environment, for completing typical tasks. However, the accuracies of the existing indoor location-tracking systems are quite unsatisfactory. Therefore, this paper introduces a high-accuracy 3D indoor positioning approach that uses a weighted nonlinear least-squares (WNLS) method. The method is tested with a set of indoor wireless sensor networks (WSNs) that employ ultra-wideband (UWB) sensors. The P440 UWB ranging and communication modules (RCMs) are utilized in this study, and both the NLS and WNLS methods are investigated. The results indicate that the WNLS method provides better positional accuracy than the NLS method, in 3D indoor positioning for a WSN employing uniform UWB sensors. Furthermore, the WNLS method can attain the reliability and robustness of the NLS method, irrespective of the configuration of WSNs. The WNLS method can be expected to improve the overall performance of 3D indoor positioning with UWB technologies. From our research, it can be concluded that WNLS can achieve more accurate positioning than NLS for a system that uses heterogeneous sensors for positioning, as long as the ranging errors between the sensors can be estimated.

Keywords: 3D indoor localization, robot, ultra-wideband, WSN

1 Introduction

1.1 Related Works

Wireless indoor localization has become a hot research topic in the recent years. In addition to the choice of sensors adopted in the system of the wireless sensor network (WSN), the use of a technique/algorithm are also important. Radio-based wireless location technologies such as Wi-Fi and Bluetooth, have been widely used for tracking a person or robot in an indoor environment [1]. Ultra-wideband (UWB) is a short-range and energy efficient radio technology that is useful in high-bandwidth wireless communication [2-3]. The ranging accuracy achieved using UWB technology is several times better than that of the traditional positioning systems based on Wi-Fi, Bluetooth, radio-frequency identification (RFID), or global positioning system (GPS) signals [4]. UWB technology has emerged as a viable candidate for use in indoor positioning approaches [5]. UWB signals also present new opportunities for indoor position tracking, owing to their ability to operate in non–line-of-sight (NLOS) conditions [6].

* Corresponding Author

This study aims to assess the performance of indoor positioning networks that use the state-of-art UWB technology.

The use of UWB sensors to build WSNs is increasing, and they are being used in a wide range of applications such as event detection, [7], target tracking [8], home automation, warehouse management, prisoner supervision, integration with other navigation information [9], earthquake rescue [10], home telehealth [11], etc. Reference [12] presented the use of UWB WSNs in improving diagnostic procedures and monitoring patients during the course of treatment. These applications were all based on location services that were widely applied in people's lives, and which had become an important part of national defense, economic construction, and social life [13].

Techniques using UWB WSNs for localization are becoming increasingly popular. In general, location determination comprises two phases—distance estimation, which is commonly referred to as ranging, and position calculation in a three-dimensional (3D) space [14]. Distance estimation can be performed by exchanging information between two nodes within a WNS. This information often includes the received signal strength indication (RSSI) [14], angle of arrival (AOA) [15-16], time of arrival (TOA) [17-18], and time difference of arrival (TDOA) [19]. In UWB WSNs, distance estimation is based on the TDOA method [20]. According to the estimated angles or distances, the 3D coordinates of a UWB sensor are computed using certain algorithms. These algorithms can be classified into four main categories [14]: geometry-based algorithms [21], cost function minimization, fingerprint [22], and Bayesian techniques [23]. The most commonly used algorithms are the geometry-based approaches [17, 24-26], which compute the position based on the estimated angles and distances, using simple algebraic relationships.

Combining the STBCS-TDOA [26] high-accuracy computing method, UWB WSNs have become one of the most promising 3D indoor positioning technologies. While several UWB positioning algorithms have been proposed, the majority of them focus on two-dimensional (2D) positioning [27-28]. As 3D positioning can provide more useful information for indoor applications, these methods would be impacted adversely and provide less positioning precision. For example, STBCS-TDOA algorithm can achieve a sub-mm accuracy, however, it is invalid when the system use ultra-low sampling rate ADCs [26]. The nonlinear least-squares (NLS) method can be used in 2D or 3D positioning, but it considers the homoscedastic case only, where all variances of ranging error must be equal and all covariances must be zero [29]. The accuracy assessment of the estimated parameters is still problematic and the variance component estimate of the ranging error is biased [30]. If the bias can be numerically estimated and removed, an unbiased accuracy estimate is achievable. Therefore, the main objective and contribution of this paper is the evaluation of the unbiased accuracy of the weighted nonlinear least-squares (WNLS) algorithms. With this purpose, we set up a realistic scenario with real UWB sensors (P440) and propose a specific UWB WSN 3D indoor positioning approach. For reducing the positioning error further, the WNLS algorithm is adopted to solve a set of equations formed using the distance relationships between each pair of P440 UWB ranging and communication modules (RCMs) in the network. The results of our experiments indicate that the WNLS method can achieve higher positioning accuracy than the conventional NLS method, while retaining similar robustness, irrespective of the specific configuration of the WSNs. It is believed that the WNLS method will improve the overall performance of 3D indoor positioning based on UWB technologies.

1.2 P440 UWB RCM

Time Domain's PulsOn 440 (P440) module is a UWB radio transceiver operating between 3.1 and 4.8 GHz. It can provide four functions (range determination, data transfer, monostatic radar, and multistatic radar) simultaneously. The ranging error in LOS conditions is in the order of a few centimeters. The P440 measures distance using a technique called two-way time of flight (TW-TOF). In this approach, the radio requesting the range measurement (the requestor) will transmit a packet of pulses that will be received by one or more units (the responders).

The 3D indoor positioning system based on P440 UWB RCMs consists of a set of five P440 modules with centimeter ranging accuracies. Four modules are used as anchors (one of which is interfaced with an external computer for user display and for running application software) and one module is used as a tag. The tag is equipped on a small robot. Fig. 1 to Fig. 3 illustrate the hardware configuration of the P440 UWB RCM system operated at a center frequency of 4.3 GHz with an instantaneous −10 dB bandwidth of 2.2 GHz. A picture of the antenna side of the tag electronics is shown in Fig. 4.

Fig. 1. P440 receiver

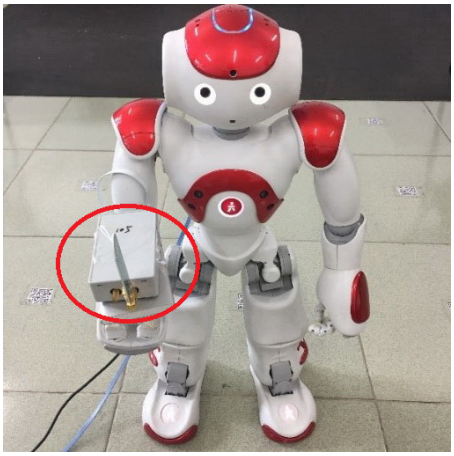

Fig. 2. P440 equipped on a robot

Fig. 3. P440 interfaced with a computer

Fig. 4. Broad-spectrum antenna side of the P440 tag

The main work and contributions of this paper can be highlighted as follows:

This paper proposes a specific UWB WSN 3D indoor positioning approach and sets up a realistic scenario with real UWB sensors (P440). For reducing the positioning error further, the WNLS algorithm is adopted to solve a set of equations formed using the distance relationships between each pair of P440 UWB ranging and communication modules (RCMs) in the network. The results of our experiments indicate that the WNLS method can achieve higher positioning accuracy than the conventional NLS method, while retaining similar robustness, irrespective of the specific configuration of the WSNs. It is believed that the WNLS method will improve the overall performance of 3D indoor positioning based on UWB technologies.

2 Location Framework for Indoor P440 UWB WSN

UWB is a promising technology for use in short-range indoor local positioning and wireless data communication [31]. It can provide a spatial resolution that allows for precise location tracking, owing to the wideband nature of the signals. UWB systems have potentially low complexity and low cost. They are capable of resisting severe multipath reflection interferences with noise-like signal properties that create little interference to other systems. Moreover, UWB technologies can overcome the power consumption and accuracy limitations of both GPS and conventional wireless local area networks (WLANs) and are more suitable for indoor location-based applications. The framework proposed in this study can be used to position the arm of the robot in an indoor environment (Fig. 5).

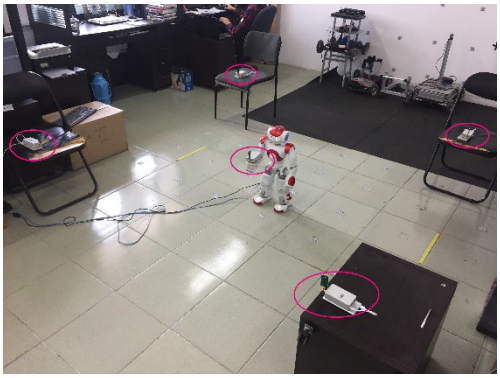

Fig. 5 UWB wireless sensor network with four reference P440 sensors and one rover P440 sensor

3 Positioning System Proposal

3.1 Distance Estimation and Position Estimation Models

To track the positions of the target nodes tagged by a P440 UWB module, the distances between each pair of P440 nodes (between the tag and an anchor or between two anchors) must be estimated. This is done through a ranging procedure. The ranging requester (tag or anchor) transmits the request to another node, which estimates the time of arrival and sends a ranging response after a predefined time. The requester measures the time of arrival of the response and can estimate the transmission delay and distance between the nodes (two-way ranging).

According to the geometrical relationship, the distance between two nodes can be written as

$$d_{tr} = \sqrt{(x_t - x_r)^2 + (y_t - y_r)^2 + (z_t - z_r)^2}\,, \tag{1}$$

where (x_t, y_t, z_t) and (x_r, y_r, z_r) are the positions of the transmitter (requester) and receptor (responder), respectively. Even if the positions of the transmitter and receptor are unknown, if the number of nodes, n, is sufficiently large and many equations similar to Eq. (1) are available to form the matrix equation, each node position can be estimated. Equation (1) can be rewritten in a form suitable for minimization as

$$\varepsilon_{rt} = (x_r - x_t)^2 + (y_r - y_t)^2 + (z_r - z_t)^2 - d_{rt}^2\,, \tag{2}$$

where ε_{rt} is a residual to be minimized simultaneously. Here, assuming that the number of nodes is n, we can obtain $n(n\text{-}1)/2$ link distance estimations with n nodes. That means $n(n\text{-}1)/2$ equations can be obtained to form an equation set. The equation set can be written in a minimized form as

$$\varepsilon_{ij} = (x_i - x_j)^2 + (y_i - y_j)^2 + (z_i - z_j)^2 - d_{ij}^2 \ (1 < i < n-1,\ i+1 < j < n), \tag{3}$$

where $\varepsilon_{ij} \equiv \boldsymbol{\varepsilon}$ is the $n(n\text{-}1)/2 \times 1$ vector of measurable links in the system, as well as the vector of residuals to be minimized simultaneously. In Eq. (3), (x_i, y_i, z_i) and (x_j, y_j, z_j) are the coordinates of the i^{th} and j^{th} nodes, respectively. We assume that the positioning dimension is l; thus, an uncertainty at a level of $l \cdot n - l \cdot (l+1)/2$ will be present in the equation set. This uncertainty is explained below. For example, when the positioning dimension is one, Eq. (3) can be rewritten as

$$\varepsilon_{ij} = (x_i - x_j)^2 - d_{ij}^2 \ (1 < i < n-1,\ i+1 < j < n). \tag{4}$$

In a one-dimensional positioning system with two nodes (one anchor and one tag), a node should be selected as the reference origin $P_1(0)$. Thus, the unknown quantity in Eq. (4) is one, which can be expressed as $n-1$. In a 2D positioning system, which consist of three nodes (two anchors and one tag), Eq. (3) can be written as

$$\varepsilon_{ij} = (x_i - x_j)^2 + (y_i - y_j)^2 - d_{ij}^2 \ (1 < i < n-1,\ i+1 < j < n). \tag{5}$$

To realize 2D positioning, a reference line with two nodes should be defined. We assume that the reference line is formed by $P_1(0,0) \leftrightarrow P_2(x,0)$. Thus, there are $2n-3$ uncertainties in Eq. (5). For the 3D positioning system, a reference plane composed of three nodes is set up and it can be assumed to be $P_1(0,0,0) \leftrightarrow P_2(x,0,0) \leftrightarrow P_3(x,y,0)$. Then, the unknown number will be $3n-6$. So forth, when the positioning dimension is l, there will be $l \cdot n - l \cdot (l+1)/2$ unknowns in Eq. (3). When the condition of Eq. (6) is satisfied, all the uncertainties in Eq. (3) can be solved.

$$\frac{n(n-1)}{2} \geq l \cdot n - \frac{l \cdot (l+1)}{2}. \tag{6}$$

Equation (3) can be further deduced to a quadratic-equation set, which is formed by n nodes and has $n(n-1)/2$ equations with $l \cdot n - l \cdot (l+1)/2$ variables. It will have two solutions, at the most. To make the solutions of the equations unique, and based on actual analysis, one more node is added in the positioning system to further determine which side space of the reference plane the positioning node is in. Finally, Eq. (6) can be revised to

$$\frac{n(n-1)}{2} > l \cdot n - \frac{l \cdot (l+1)}{2}. \tag{7}$$

Thus, the positioning issue becomes a problem of solving a set of nonlinear equations, which specifically have $l \cdot n - l \cdot (l+1)/2$ variables and a unique solution.

3.2 Position Estimation Algorithms of Weighted and Unweighted Nonlinear Least Squares

According to the optimization solution theory, there are many methods to solve the problem of a set of nonlinear equations such as Eq. (3). In this work, the Gauss–Newton iteration method is used for the simultaneous minimization of a set of nonlinear equations. We provide a brief derivation of the mathematical framework involved in combining the distances between each pair of nodes in a set of nodes, followed by an experimental example using five nodes. Each node is assumed to be within the range of all other nodes, providing full link distances for ten links. These equations can be rewritten in a form suited for minimization, as in Eq. (8).

$$\varepsilon_{ij} = (x_i - x_j)^2 + (y_i - y_j)^2 + (z_i - z_j)^2 - d_{ij}^2 \ (1 < i < 4,\ i+1 < j < 5). \tag{8}$$

The Gauss–Newton iteration method requires linearization of the equations using the first-order Taylor's expansion. At the heart sits a Jacobian matrix **J** that can be obtained by taking the partial derivatives of all equations with respect to all unknowns. The gradient equation requires inverting the Jacobian, when applied to large numbers of nodes. Matrix inversion should be concerned the computational complexity prompting for speed. While higher-speed computation is available with the recently developed techniques, the computing speed issue need not be focused on much, because the auto-survey process is targeted at the localization of static nodes in a central base station. Most real-world applications will not require a high density of anchor nodes and/or link distances. Our sample Jacobian, developed for a five-node system with ten measurable links, is

$$\mathbf{J}=\begin{pmatrix}
\frac{\partial \varepsilon_{12}}{\partial x_2} & \frac{\partial \varepsilon_{12}}{\partial x_3} & \frac{\partial \varepsilon_{12}}{\partial y_3} & \frac{\partial \varepsilon_{12}}{\partial x_4} & \frac{\partial \varepsilon_{12}}{\partial y_4} & \frac{\partial \varepsilon_{12}}{\partial z_4} & \frac{\partial \varepsilon_{12}}{\partial x_5} & \frac{\partial \varepsilon_{12}}{\partial y_5} & \frac{\partial \varepsilon_{12}}{\partial z_5} \\
\frac{\partial \varepsilon_{13}}{\partial x_2} & \frac{\partial \varepsilon_{13}}{\partial x_3} & \frac{\partial \varepsilon_{13}}{\partial y_3} & \frac{\partial \varepsilon_{13}}{\partial x_4} & \frac{\partial \varepsilon_{13}}{\partial y_4} & \frac{\partial \varepsilon_{13}}{\partial z_4} & \frac{\partial \varepsilon_{13}}{\partial x_5} & \frac{\partial \varepsilon_{13}}{\partial y_5} & \frac{\partial \varepsilon_{13}}{\partial z_5} \\
\frac{\partial \varepsilon_{14}}{\partial x_2} & \frac{\partial \varepsilon_{14}}{\partial x_3} & \frac{\partial \varepsilon_{14}}{\partial y_3} & \frac{\partial \varepsilon_{14}}{\partial x_4} & \frac{\partial \varepsilon_{14}}{\partial y_4} & \frac{\partial \varepsilon_{14}}{\partial z_4} & \frac{\partial \varepsilon_{14}}{\partial x_5} & \frac{\partial \varepsilon_{14}}{\partial y_5} & \frac{\partial \varepsilon_{14}}{\partial z_5} \\
\frac{\partial \varepsilon_{15}}{\partial x_2} & \frac{\partial \varepsilon_{15}}{\partial x_3} & \frac{\partial \varepsilon_{15}}{\partial y_3} & \frac{\partial \varepsilon_{15}}{\partial x_4} & \frac{\partial \varepsilon_{15}}{\partial y_4} & \frac{\partial \varepsilon_{15}}{\partial z_4} & \frac{\partial \varepsilon_{15}}{\partial x_5} & \frac{\partial \varepsilon_{15}}{\partial y_5} & \frac{\partial \varepsilon_{15}}{\partial z_5} \\
\frac{\partial \varepsilon_{23}}{\partial x_2} & \frac{\partial \varepsilon_{23}}{\partial x_3} & \frac{\partial \varepsilon_{23}}{\partial y_3} & \frac{\partial \varepsilon_{23}}{\partial x_4} & \frac{\partial \varepsilon_{23}}{\partial y_4} & \frac{\partial \varepsilon_{23}}{\partial z_4} & \frac{\partial \varepsilon_{23}}{\partial x_5} & \frac{\partial \varepsilon_{23}}{\partial y_5} & \frac{\partial \varepsilon_{23}}{\partial z_5} \\
\frac{\partial \varepsilon_{24}}{\partial x_2} & \frac{\partial \varepsilon_{24}}{\partial x_3} & \frac{\partial \varepsilon_{24}}{\partial y_3} & \frac{\partial \varepsilon_{24}}{\partial x_4} & \frac{\partial \varepsilon_{24}}{\partial y_4} & \frac{\partial \varepsilon_{24}}{\partial z_4} & \frac{\partial \varepsilon_{24}}{\partial x_5} & \frac{\partial \varepsilon_{24}}{\partial y_5} & \frac{\partial \varepsilon_{24}}{\partial z_5} \\
\frac{\partial \varepsilon_{25}}{\partial x_2} & \frac{\partial \varepsilon_{25}}{\partial x_3} & \frac{\partial \varepsilon_{25}}{\partial y_3} & \frac{\partial \varepsilon_{25}}{\partial x_4} & \frac{\partial \varepsilon_{25}}{\partial y_4} & \frac{\partial \varepsilon_{25}}{\partial z_4} & \frac{\partial \varepsilon_{25}}{\partial x_5} & \frac{\partial \varepsilon_{25}}{\partial y_5} & \frac{\partial \varepsilon_{25}}{\partial z_5} \\
\frac{\partial \varepsilon_{34}}{\partial x_2} & \frac{\partial \varepsilon_{34}}{\partial x_3} & \frac{\partial \varepsilon_{34}}{\partial y_3} & \frac{\partial \varepsilon_{34}}{\partial x_4} & \frac{\partial \varepsilon_{34}}{\partial y_4} & \frac{\partial \varepsilon_{34}}{\partial z_4} & \frac{\partial \varepsilon_{34}}{\partial x_5} & \frac{\partial \varepsilon_{34}}{\partial y_5} & \frac{\partial \varepsilon_{34}}{\partial z_5} \\
\frac{\partial \varepsilon_{35}}{\partial x_2} & \frac{\partial \varepsilon_{35}}{\partial x_3} & \frac{\partial \varepsilon_{35}}{\partial y_3} & \frac{\partial \varepsilon_{35}}{\partial x_4} & \frac{\partial \varepsilon_{35}}{\partial y_4} & \frac{\partial \varepsilon_{35}}{\partial z_4} & \frac{\partial \varepsilon_{35}}{\partial x_5} & \frac{\partial \varepsilon_{35}}{\partial y_5} & \frac{\partial \varepsilon_{35}}{\partial z_5} \\
\frac{\partial \varepsilon_{45}}{\partial x_2} & \frac{\partial \varepsilon_{45}}{\partial x_3} & \frac{\partial \varepsilon_{45}}{\partial y_3} & \frac{\partial \varepsilon_{45}}{\partial x_4} & \frac{\partial \varepsilon_{45}}{\partial y_4} & \frac{\partial \varepsilon_{45}}{\partial z_4} & \frac{\partial \varepsilon_{45}}{\partial x_5} & \frac{\partial \varepsilon_{45}}{\partial y_5} & \frac{\partial \varepsilon_{45}}{\partial z_5}
\end{pmatrix}. \tag{9}$$

The Jacobian matrix can be specifically written as

$$\mathbf{J}=\begin{pmatrix}
2(x_2-x_1) & 0 & 0 & 0 & 0 & 0 & 0 & 0 & 0 \\
0 & 2(x_3-x_1) & 2(y_3-y_1) & 0 & 0 & 0 & 0 & 0 & 0 \\
0 & 0 & 0 & 2(x_4-x_1) & 2(y_4-y_1) & 2(z_4-z_1) & 0 & 0 & 0 \\
0 & 0 & 0 & 0 & 0 & 0 & 2(x_5-x_1) & 2(y_5-y_1) & 2(z_5-z_1) \\
-2(x_3-x_2) & 2(x_3-x_2) & 2(y_3-y_2) & 0 & 0 & 0 & 0 & 0 & 0 \\
-2(x_4-x_2) & 0 & 0 & 2(x_4-x_2) & 2(y_4-y_2) & 2(z_4-z_2) & 0 & 0 & 0 \\
-2(x_5-x_2) & 0 & 0 & 0 & 0 & 0 & 2(x_5-x_2) & 2(y_5-y_2) & 2(z_5-z_2) \\
0 & -2(x_4-x_3) & -2(y_4-y_3) & 2(x_4-x_3) & 2(y_4-y_3) & 2(z_4-z_3) & 0 & 0 & 0 \\
0 & -2(x_5-x_3) & -2(y_5-y_3) & 0 & 0 & 0 & 2(x_5-x_3) & 2(y_5-y_3) & 2(z_5-z_3) \\
0 & 0 & 0 & -2(x_5-x_4) & -2(y_5-y_4) & -2(z_5-z_4) & 2(x_5-x_4) & 2(y_5-y_4) & 2(z_5-z_4)
\end{pmatrix}. \tag{10}$$

The equation set formed by a fully 3D five-node positioning system contains 15 unknowns. Since the reference plane is defined by $P_1(0,0,0) \leftrightarrow P_2(x,0,0) \leftrightarrow P_3(x,y,0)$, the number of unknowns is reduced to nine, which is calculated by $3n-6$. These nine unknowns can be written as a vector $X=[x_2,x_3,y_3,x_4,y_4,z_4,x_5,y_5,z_5]^T$. Here, we assume that $\mathrm{P}_1(x_1,y_1,z_1)$ is at the origin $(0,0,0)$; $\mathrm{P}_2(x_2,y_2,z_2)$ is $(x_2,0,0)$, which links with $\mathrm{P}_1(0,0,0)$ to define the direction of the x-axis; and $\mathrm{P}_3(x_3,y_3,z_3)$ is $(x_3,y_3,0)$, which combines $\mathrm{P}_1(0,0,0)$ and $\mathrm{P}_2(x_2,0,0)$ to form the reference plane. The overall objective is to develop a Jacobian with full rank, which corresponds with the actual analysis mentioned above this section. Continuing with the NLS algorithm, a "shift vector," $\mathbf{H}$, is solved in each iteration of the Gauss–Newton minimization process

$$\mathbf{H}=[\mathbf{J}^T\mathbf{J}]^{-1}\mathbf{J}^T\boldsymbol{\varepsilon}, \tag{11}$$

where $\boldsymbol{\varepsilon}$ is the residual vector.

$$\boldsymbol{\varepsilon}=[\varepsilon_{12},\varepsilon_{13},\varepsilon_{14},\varepsilon_{15},\varepsilon_{23},\varepsilon_{24},\varepsilon_{25},\varepsilon_{34},\varepsilon_{35},\varepsilon_{45}]^T. \tag{12}$$

Finally, the NLS algorithm updates the unknowns $\hat{X} = [\hat{x}_2, \hat{x}_3, \hat{y}_3, \hat{x}_4, \hat{y}_4, \hat{z}_4, \hat{x}_5, \hat{y}_5, \hat{z}_5]^{'}$ in each iteration k using

$$\hat{\mathbf{X}}^{(k+1)} = \hat{\mathbf{X}}^{(k)} - \mathbf{H}^{(k)}. \tag{13}$$

The algorithm below summarizes the NLS algorithm procedure.

Algorithm. Non-linear Least Squares (NLS)

1. Start with an initial guess or "seed point" $\hat{\mathbf{X}}$ and measurements d_{ij}.
2. Solve for $\varepsilon_{ij} = (x_i - x_j)^2 + (y_i - y_j)^2 + (z_i - z_j)^2 - d_{ij}^2$ $(1 < i < 4,\ i+1 < j < 5)$.
3. Compute the Jacobian $\mathbf{J}$.
4. Compute the shift vector $\mathbf{H}$.
5. Subtract $\mathbf{H}$ from the vector of unknowns $\hat{X} = [\hat{x}_2, \hat{x}_3, \hat{y}_3, \hat{x}_4, \hat{y}_4, \hat{z}_4, \hat{x}_5, \hat{y}_5, \hat{z}_5]^T$.
6. Repeat from step 2 until the vector norm of $\mathbf{H}$, $\|\mathbf{H}\|$, is very small, typically 0.0001 or less.

For the WNLS algorithm, the "shift vector" $\mathbf{H}_w$, is written as

$$\mathbf{H}_w = [\mathbf{J}^T \mathbf{W} \mathbf{J}]^{-1} \mathbf{J}^T \mathbf{W} \boldsymbol{\varepsilon}, \tag{14}$$

$$\mathbf{W} = \left\{1/\sigma^2\right\}_{\frac{n(n-1)}{2} \times \frac{n(n-1)}{2}}, \tag{15}$$

In Eq. (15), σ^2 is the variance of the error of P440's ranging and $\mathbf{W}$ is a diagonal matrix whose diagonal elements are the variances of the ranging errors. The steps for solving the WNLS are the same as those of the NLS algorithm, except that the initialization of $\mathbf{W}$ is added in the first step.

The algorithm below summarizes the WNLS algorithm procedure.

Algorithm. Weighted Non-linear Least Squares (WNLS)

1. Start with an initial guess or "seed point" $\hat{\mathbf{X}}$ and measurements d_{ij}.
2. Solve for $\varepsilon_{ij} = (x_i - x_j)^2 + (y_i - y_j)^2 + (z_i - z_j)^2 - d_{ij}^2$ $(1 < i < 4,\ i+1 < j < 5)$.
3. Compute the Jacobian $\mathbf{J}$.
4. Compute the shift vector $\mathbf{H}_w$.
5. Subtract $\mathbf{H}_w$ from the vector of unknowns $\hat{X} = [\hat{x}_2, \hat{x}_3, \hat{y}_3, \hat{x}_4, \hat{y}_4, \hat{z}_4, \hat{x}_5, \hat{y}_5, \hat{z}_5]^T$.
6. Repeat from step 2 until the vector norm of $\mathbf{H}_w$, $\|\mathbf{H}_w\|$, is very small, typically 0.0001 or less.

The WNLS multivariable regression approach is summarized in the flowchart shown in Fig. 6.

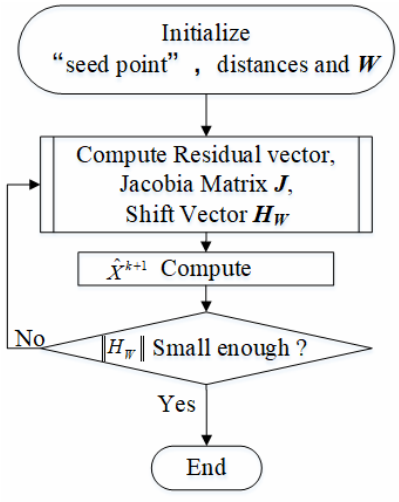

Fig. 6. Flow chart of the WNLS multivariable regression approach

4 Experiment

The coordinates of the five nodes were set up as $P_1(0,0,0)$, $P_2(8,0,0)$, $P_3(0,8,0)$, $P_4(0,0,8)$ and $P_5(4,4,4)$ in our 3D simulation. The real distances between each pair of nodes are listed in Table 1. The ranging errors associated with the different node-to-node distances of the UWB sensors should be taken into account, in practice.

Table 1. Real values of the node-to-node distances

Node-to-node	d12	d13	d14	d15	d23	d24	d25	d34	d35	d45
Real distance (m)	8.00	8.00	8.00	6.93	11.31	11.31	6.93	11.31	6.93	6.93

4.1 Positioning Result

The function-precision range measurements (PRMs) of P440 were taken using the TW-TOF ranging technique, which typically has high accuracy, and were provided with estimates of the range error. Fig. 7 shows the relationship between the estimated range error and the range obtained in a laboratory environment. The accuracy of the range measurement depends primarily on how successfully the receiving radio estimates the precise TOA of the arriving pulse through equivalent-time sampling. Diversity of estimation range error existed in the node-to-node distances of the P440 WSN. An estimate of error was provided by the requesting radio with each range measurement, in support of the weighting factors for online positioning and navigation. The standard deviation of the error and error satisfied Eq. (16).

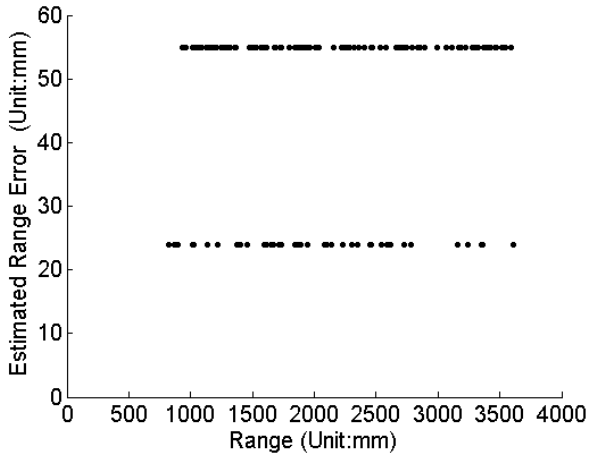

Fig. 7. Relationship between the estimated range error and range obtained in a laboratory environment

$$\delta = C\sigma . \tag{16}$$

In Eq. (16), δ is the range error, σ is the standard deviation of range error, and C is a constant indicating the level of confidence. The relationship between the confidence level and the constant C is shown in Table 2. C=2.58 was used in our experiment.

Table 2. Confidence level and constant

Confidence level	C
90%	1.64
95%	1.96
99%	2.58

Assuming that the range errors fit a Gaussian distribution with zero mean and variance σ^2, we simulated the process of positioning with NLS and WNLS methods after adding Gaussian random errors that retained a mean of zero and a standard deviation σ ($\delta = C\sigma$ and δ is shown in Table 3.). Fig. 8 shows the rover node positioning result when the diversity of the estimation range error is not considered. It is obvious that the NLS and WNLS methods achieve identical positioning accuracies. However, the positioning result will be different when diversity exists in the estimated range errors. This is because the ranging accuracy of the node-to-node distance is not consistent. As a result, the residual vector cannot be normalized to a unit diagonal matrix, which can also be verified by Eq. (14). Fig. 9 shows the positioning result when the estimated range error is considered in the positioning experiment. The positional differences corresponding to the NLS and WNLS methods can be clearly identified in Fig. 9. However, both methods retain the same stability and robustness for the same number of iterations. The next subsection analyzes the error in detail.

Table 3. Possible estimated ranging errors of node-to-node pairs. (Unit: mm)

Node-to-node range error	δ_{12}	δ_{13}	δ_{14}	δ_{15}	δ_{23}	δ_{24}	δ_{25}	δ_{34}	δ_{35}	δ_{45}
First experiment	22	55	55	55	55	55	55	55	55	55
Second experiment	22	22	55	55	55	55	55	55	55	55
Third experiment	22	22	22	55	55	55	55	55	55	55
Fourth experiment	22	22	22	22	55	55	55	55	55	55
Fifth experiment	22	22	22	22	22	55	55	55	55	55
Sixth experiment	22	22	22	22	22	22	55	55	55	55
Seventh experiment	22	22	22	22	22	22	22	55	55	55
Eighth experiment	22	22	22	22	22	22	22	22	55	55
Ninth experiment	22	22	22	22	22	22	22	22	22	55

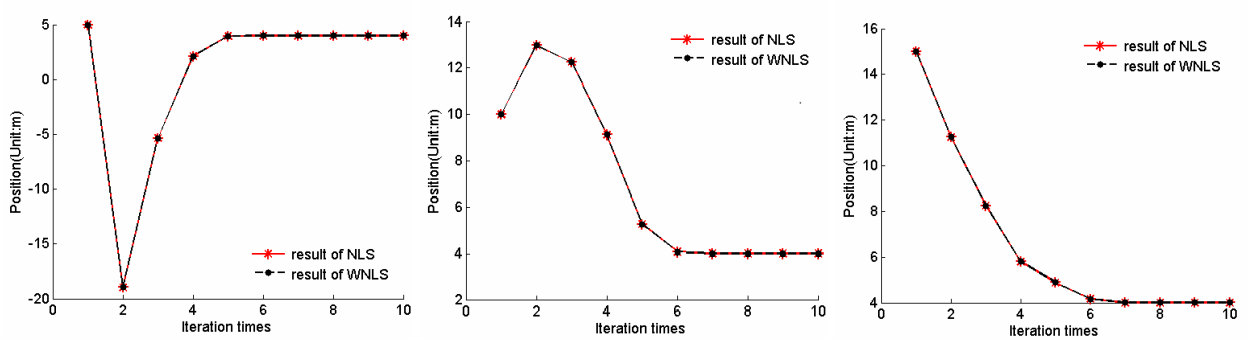

(a) Node 5 along X direction (b) Node 5 along Y direction (c) Node 5 along Z direction

Fig. 8. Rover node positioning result for a constant range error

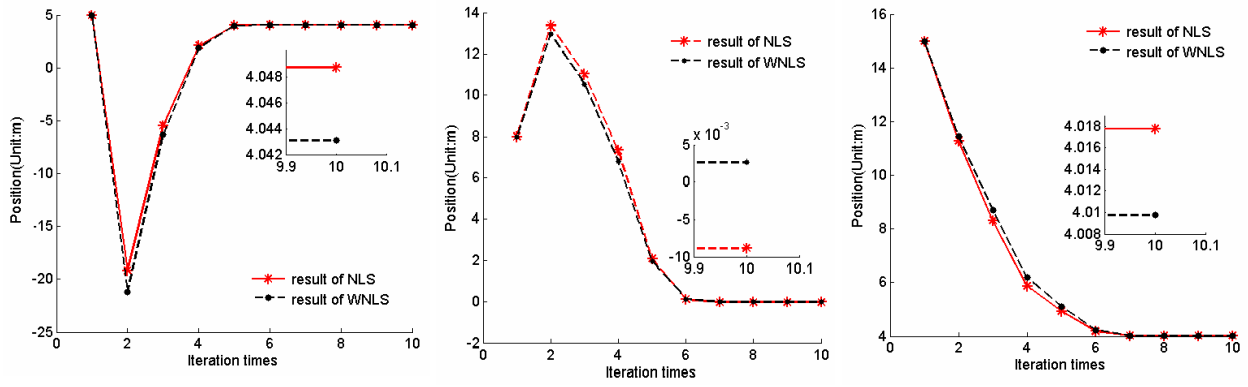

(a) Node 5 along X direction (b) Node 5 along Y direction (c) Node 5 along Z direction

Fig. 9. Rover node positioning result for diverse range errors

4.2 Error Comparison Experiment

We conducted nine sets of experiments to verify the positioning error of the NLS and WNLS methods. In each experiment, we performed 1000 positioning tests for both the methods. Each test added random errors to the real distances. We assumed that the estimated range error for each node-to-node pair was different. In the first experiment, one estimated range error of a node-to-node pair was 0.022 m and the other estimated range errors were 0.055 m. Here, we assumed that the estimated range error δ_{12} between node no. 1 and node no. 2 was 0.022 m. In the second experiment, two estimated range errors of node-to-node pairs were 0.022 m and the other estimated range errors were 0.055 m. Here, we assumed that the estimated range errors δ_{12} and δ_{13} were 0.022 m. So on, in the ninth experiment, seven estimated range errors of node-to-node pairs were 0.022 m and only one estimated range error was 0.055 m. The possible estimated range errors of our nine experiments are shown in Table 3. The rover P440 positioning accuracy result is shown in Table 4.

Table 4. Positioning accuracy and percentage of accuracy improvement

	1st	2nd	3rd	4th	5th	6th	7th	8th	9th
NLS (mm)	71.6	72.3	70.3	42.6	40.0	38.6	34.7	34.2	32.2
WNLS (mm)	50.7	51.3	50.1	22.0	21.5	21.6	20.8	22.0	21.3
Percentage (%)	29.19	29.05	28.73	48.25	46.25	44.04	40.06	35.67	33.85

Finally, we obtained the positioning errors corresponding to these two methods. Figures 10 to 18 show the positioning results and the range error statistics for these nine experiments. The subfigures (a) of Fig. 10 to Fig. 18 show the positioning errors of each experiment with NLS and WNLS methods, and the subfigures (b) of Fig. 10 to Fig. 18 illustrate the probability densities of the range errors. The black and

red dotted vertical lines indicate the positioning errors of the NLS and WNLS methods, respectively. Through these nine experiments, we can see from Table 4 that different estimated range errors have a great influence on the rover node positioning error, but WNLS method can improve the positioning accuracy by more than 28%. Especially, when the differentiation of the estimated range errors is particularly large, the rover node positioning accuracy can be increased by more than 48%.

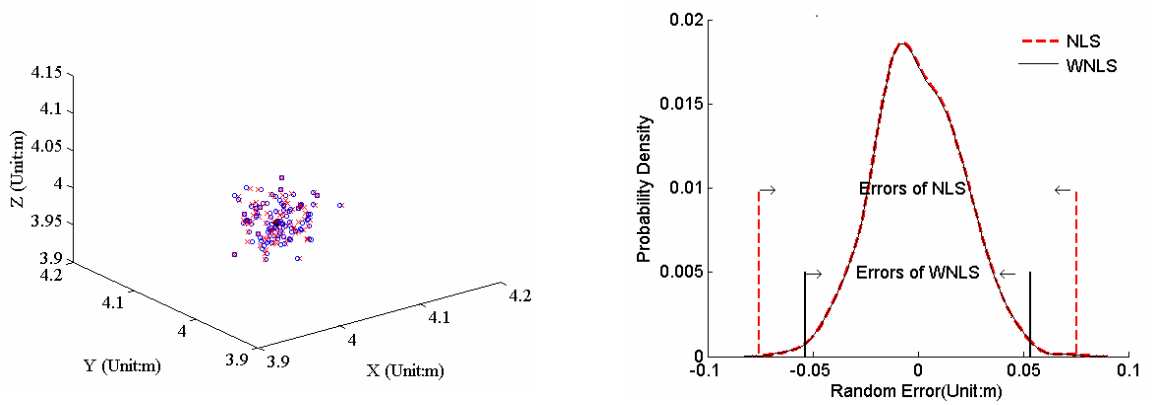

(a) Positioning result (b) Error statistics result

Fig. 10. Positioning error result of the first experiment

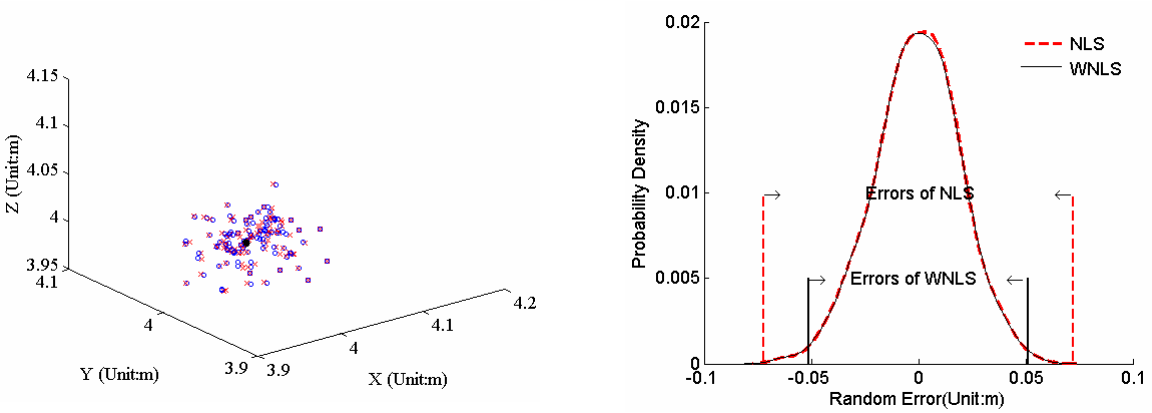

(a) Positioning result (b) error statistics result

Fig. 11. Positioning error result of the second experiment

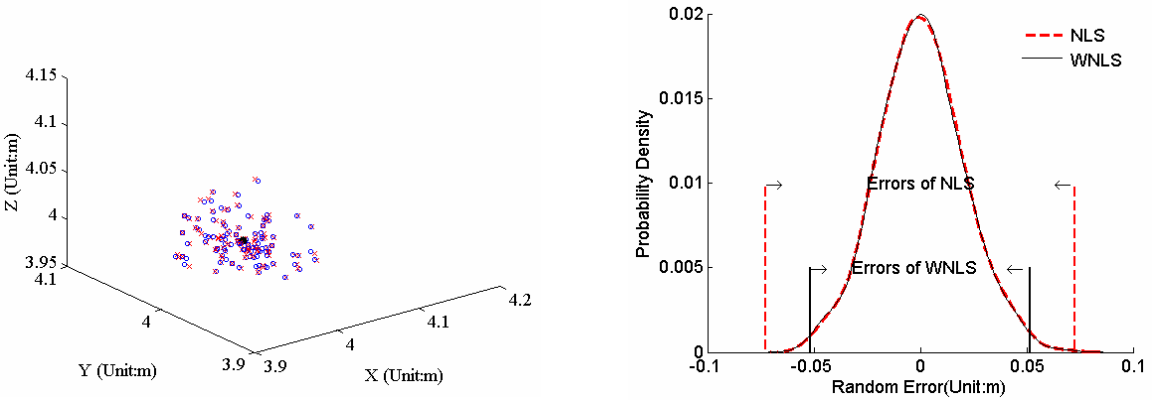

(a) Positioning result (b) Error statistics result

Fig. 12. Positioning error result of the third experiment

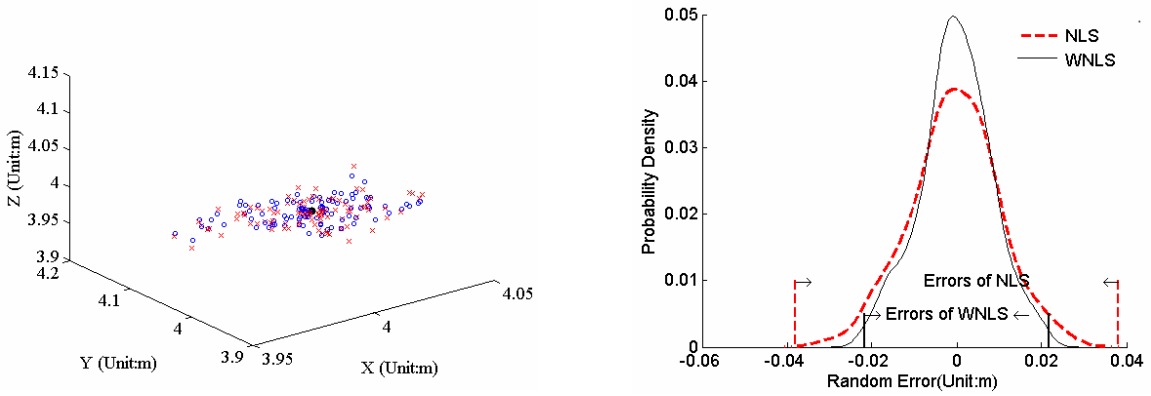

(a) Positioning result (b) Error statistics result

Fig. 13. Positioning error result of the fourth experiment

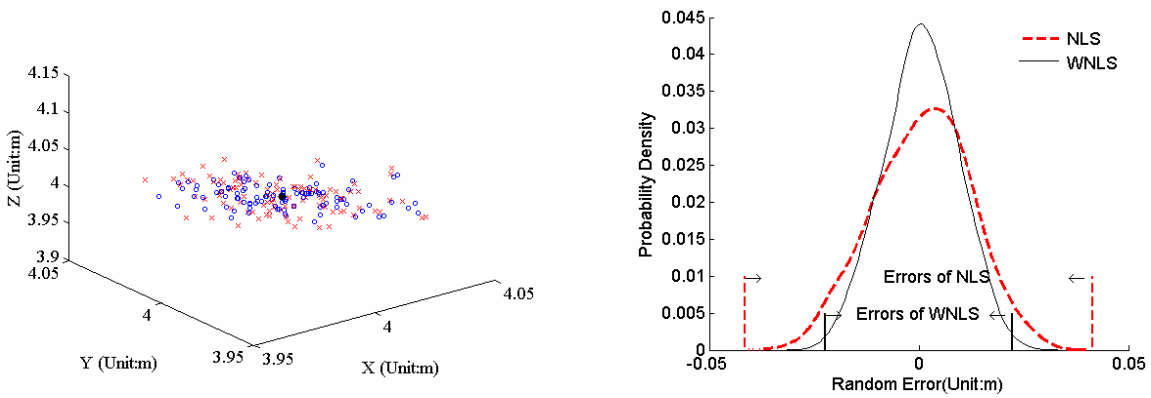

(a) Positioning result (b) Error statistics result

Fig. 14. Positioning error result of the fifth experiment

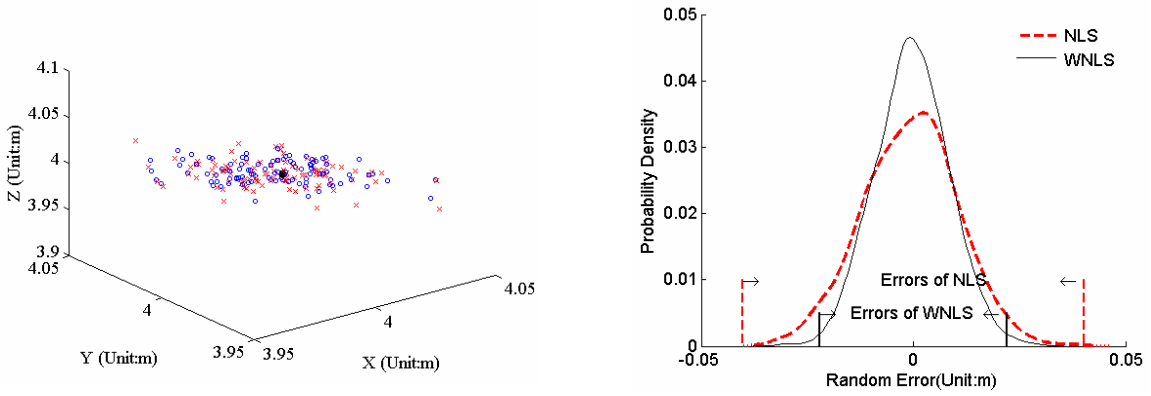

(a) Positioning result (b) Error statistics result

Fig. 15. Positioning error result of the sixth experiment

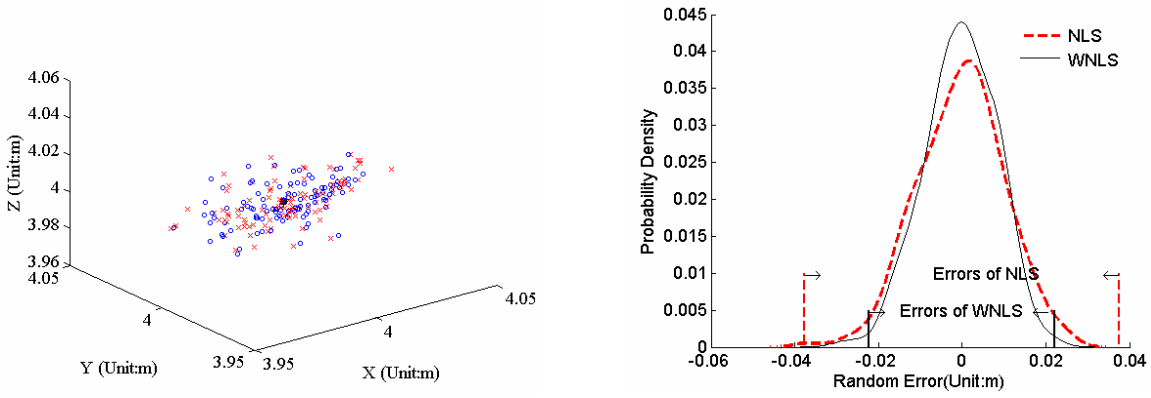

(a) Positioning result (b) error statistics result

Fig. 16. Positioning error result of the seventh experiment

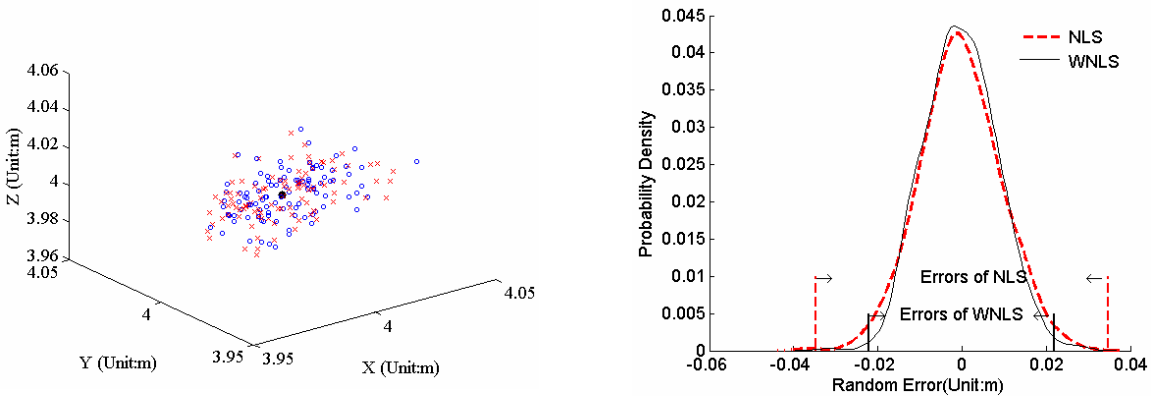

(a) Positioning result (b) error statistics result

Fig. 17. Positioning error result of the eighth experiment

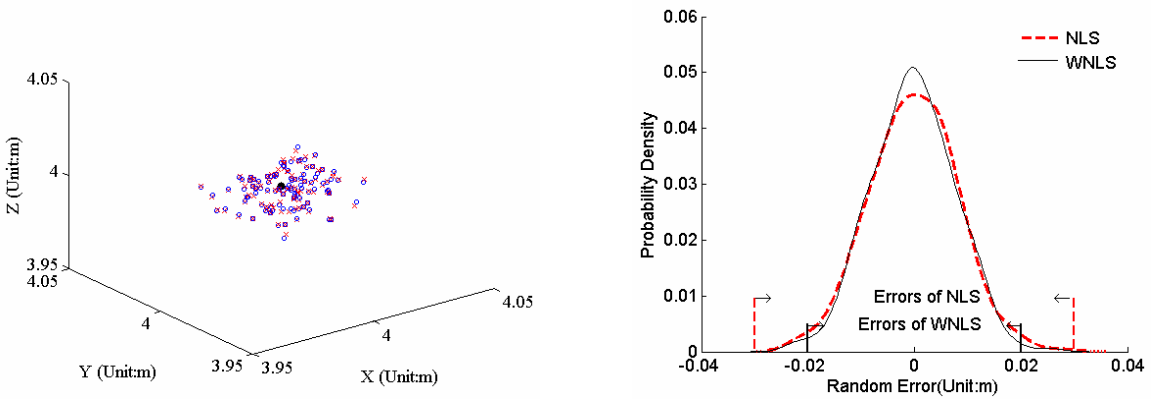

(a) Positioning result (b) error statistics result

Fig. 18. Positioning error result of the ninth experiment

All models of the P440 UWB sensors utilized in this experiment were similar. However, from our research results, it can be concluded that, when the system uses heterogeneous sensors for positioning, as long as the ranging errors between the heterogeneous sensors can be estimated, good positioning results can be obtained.

5 Conclusion

P440 RCMs have different estimated accuracies when used for ranging, which will increase the positioning error. From the experimental results, it can be proved that the WNLS method exhibits obvious improvement in the positioning precision under the premise of ensured stability and robustness of the system. This method can serve as a good reference for the integration of complex systems, in the future. We are confident that, with the proposed future work, our design can be adapted to a home-like environment with more robust localization and higher accuracy solution. This method utilizes the real-time distance error estimation parameters provided by P440 to realize the high accuracy positioning and it is not valid in the system that cannot estimate distance error parameters.

Acknowledgements

This project was supported by the National Science Foundation of China (No. 61501019), Scientific Research Project of the Beijing Educational Committee (No. SQKM201710016008), Open Research Fund Program of the Beijing Key Laboratory of Robot Bionics and Function Research (No. 07080915001), Research Fund for the Doctoral Program of the Beijing University of Civil Engineering and Architecture, and Fundamental Research Funds for the Beijing University of Civil Engineering and Architecture (No. 18209).

References

[1] P.K. Yoon, S. Zihajehzadeh, B.S. Kang, E.J. Park, Robust biomechanical model-based 3-D indoor localization and tracking method using UWB and IMU, IEEE Sens. J. 17(4)(2017) 1084-1096.

[2] B. Jachimczyk, D. Dziak, W.J. Kulesza, Customization of UWB 3D-RTLS based on the new uncertainty model of the AoA ranging technique, Sensors (Switzerland) 17(2)(2017) 227.

[3] S. Maranò, W.M. Gifford, H. Wymeersch, M.Z. Win, NLOS identification and mitigation for localization based on UWB experimental data, IEEE J. Sel. Areas Commun 28(7)(2010) 1026-1035.

[4] R.J. Fontana, E. Richley, J. Barney, Commercialization of an ultra wideband precision asset location system, in: Proc. 2003 IEEE Conf. Ultra Wideband Syst. Technol, 2003.

[5] F. Mazhar, M.G. Khan, B. Sällberg, Precise indoor positioning using UWB: a review of methods, algorithms and implementations, Wirel. Pers. Commun. 97(3)(2017) 4467-4491.

[6] W. Suski, S. Banerjee, A. Hoover, Using a map of measurement noise to improve UWB indoor position tracking, IEEE Trans. Instrum. Meas. 62(8)(2013) 2228-2236.

[7] G. Naddafzadeh-Shirazi, L. Lampe, Lifetime maximization in UWB sensor networks for event detection, IEEE Trans. Signal Process 59(9)(2011) 4411-4423.

[8] W. Suski, A study of environment noise in ultra-wideband indoor position tracking, [dissertation] Clemson, SC: Clemson University, 2012.

[9] S. Li, G. Li, L. Wang, Y. Zhou, Y. Peng, J. Fu, A three-dimensional robust ridge estimation positioning method for UWB in a complex environment, Adv. Sp. Res. 60(12)(2017) 2763-2775.

[10] L. Zhang, C.-C. Lim, Y. Chen, H.R. Karimi, Tracking mobile robot in indoor wireless sensor networks, Math. Probl. Eng. 2014(2)(2014) 837050.

[11] T. Paget, C. Jones, M. Davies, C. Evered, C. Lewis, Using home telehealth to empower patients to monitor and manage long term conditions, Nurs. Times 106(45)(2010) 17-19.

[12] A.S. Dmitriev, A.I. Ryzhov, V.A. Lazarev, N.V. Malyutin, G.K. Mansurov, M.G. Popov, Experimental ultrawideband wireless sensor network for medical applications, J. Commun. Technol. Electron. 60(9)(2015) 1027-1036.

[13] Z. Deng, Y. Yu, X. Yuan, N. Wan, L. Yang, Situation and development tendency of indoor positioning, China Commun. 10(3)(2013) 42-55.

[14] J. Choliz, M. Eguizabal, A. Hernandez-Solana, A. Valdovinos, Comparison of algorithms for UWB indoor location and tracking systems, in: Proc. IEEE 73rd Veh. Technol. Conf. VTC Spring, 2011.

[15] J. Xu, M. Ma, C.L. Law, AOA cooperative position localization, in: Proc. GLOBECOM - IEEE Glob. Telecommun. Conf., 2008.

[16] P. Kułakowski, J. Vales-Alonso, E. Egea-López, W. Ludwin, J. García-Haro, Angle-of-arrival localization based on antenna arrays for wireless sensor networks, Comput. Electr. Eng. 36(6)(2010) 1181-1186.

[17] G. Cheng, Accurate TOA-based UWB localization system in coal mine based on WSN, Phys. Procedia 24(A)(2012) 534-540.

[18] Y. Jiang, Q. Hu, D. Yang, Analysis of positioning error for two-dimensional location system, Math. Probl. Eng. 2013(2013) 163958.

[19] C.H. N. Reddy, M.B.R. Sujatha, TDOA computation using multicarrier modulation for sensor networks, Int. J. Comput. Sci. Commun. Netw. 1(1)(2011) 85-90.

[20] A. Alarifi, A. Al-Salman, M. Alsaleh, A. Alnafessah, S. Al-Hadhrami, M.A. Al-Ammar, H.S. Al-Khalifa, Ultra wideband indoor positioning technologies: analysis and recent advances, Sensors 16(5)(2016) E707.

[21] K.W. Cheung, H.C. So, W.K. Ma, Y.T. Chan, Least squares algorithms for time-of-arrival-based mobile location, IEEE Trans. Signal Process. 52(4)(2004) 1121-1130.

[22] K. Kaemarungsi, P. Krishnamurthy, Modeling of indoor positioning systems based on location fingerprinting, INFOCOM 2004. Twenty-third Annu. Conf. IEEE Comput. Commun. Soc. 00(C)(2004) 1012-1022.

[23] V. Fox, J. Hightower, L. Liao, D. Schulz, G. Borriello, Bayesian filtering for location estimation, IEEE Pervasive Comput. 2(3)(2003) 24-33.

[24] E. Arias-De-Reyna, U. Mengali, A maximum likelihood UWB localization algorithm exploiting knowledge of the service area layout, Wirel. Pers. Commun. 69(4)(2013) 1413-1426.

[25] L. Mucchi, F. Trippi, A. Carpini, Ultra wide band real-time location system for cinematic survey in sports, in: Proc. 3rd Int. Symp. Appl. Sci. Biomed. Commun. Technol. ISABEL, 2010.

[26] D. Yang, H. Li, Z. Zhang, G.D. Peterson, Compressive sensing based sub-mm accuracy UWB positioning systems: a space-time approach, Digit. Signal Process. A Rev. J. 23(1)(2013) 340-354.

[27] P. Muller, H. Wymeersch, R. Piche, UWB positioning with generalized Gaussian mixture filters, IEEE Trans. Mob. Comput. 13(10)(2014) 2406-2414.

[28] E. Garcia, P. Poudereux, A. Hernandez, J. Urena, D. Gualda, A robust UWB indoor positioning system for highly complex environments, in: Proc. IEEE Int. Conf. Ind. Technol. 2015.

[29] B. Schaffrin, A. Wieser, On weighted total least-squares adjustment for linear regression, J. Geod. 82(7)(2008) 415-421.

[30] Y. Shen, B. Li, Y. Chen, An iterative solution of weighted total least-squares adjustment, J. Geod. 85(4)(2011) 229-238.

[31] C. Zhang, M.J. Kuhn, B.C. Merkl; A.E. Fathy, M.R. Mahfouz, Realtime non-coherent UWB positioning radar with millimeter range accuracy: theory and experiment, IEEE Trans. Microw. Theory Tech. 58(1)(2010) 9-20.